Modeling Passive Mechanical Interaction between Aqueous Humor and Iris

Jeffrey J. Heys[1], Victor H. Barocas[2]* and Michael J. Taravella[3]

[1]Department of Chemical Engineering

University of Colorado, Boulder, CO 80309-0424

[2]Department of Biomedical Engineering

University of Minnesota, Minneapolis, MN 55455

[3]Department of Ophthalmology

University of Colorado Health Sciences Center, Denver, CO 80262

*corresponding author (tel: 612-626-5572; fax: 612-626-6583; email: *baroc001@umn.edu)*

Keywords: eye, finite element method, iris bomb

Abstract

We present a mathematical model of the coupled aqueous humor —iris system that accounts for the contribution of aqueous humor flow and passive iris deformability to the iris contour. The aqueous humor is modeled as a Newtonian fluid, and the iris is modeled as a linear elastic solid. The resulting coupled equation set is solved by the finite element method with mesh motion in response to iris displacement accomplished by tracking a pseudo-solid overlying the aqueous humor. The model is used to predict the iris contour and intraocular pressure in healthy eye with varying pupil diameter, as well as during blinking; iris bomb ,which is characterized by dramatic bulging of the iris, is also considered. The results compare favorably with clinical observations, supporting the hypothesis that passive iris deformation can produce the pathological contours.

Introduction

Glaucoma affects millions of Americans and is the second leading cause of blindness worldwide [1]. As a result, there has been much experimental and clinical research on glaucoma [2]. It has only been in the last thirty years that theoretical models have been developed to study glaucoma. While there are still computational limitations in the level of complexity possible when modeling the eye, we present a natural extension of the previous theoretical work, especially that of Tiedmann [3] and Friedland [4]. The new model predicts the flow profile of aqueous humor through the anterior eye and the contour (or displacement) of the iris resulting from both the pressure drop and the shear stress due to that flow.

Aqueous humor (AH) is the transparent fluid that circulates through the anterior chamber and provides nutrition for avascular ocular tissues (i.e., the lens, cornea, trabecular meshwork, and anterior vitreous, see Fig. 1). The AH is actively secreted by the ciliary processes into the posterior chamber, passes through the pupil, enters the anterior chamber, and eventually exits, primarily through the trabecular meshwork. The uveoscleral outflow route near the trabecular meshwork accounts for less than 20% of the total outflow [5]. The third possible exit route, accounting for a small fraction of the outflow of AH in healthy eyes, is through the vitreous gel and retina [6], which is immediately posterior to the lens and the posterior chamber. AH is secreted at a rate of approximately 1.5-3.0 μL/min, which results in a residence time of approximately 100 minutes [7, 8]. All but a small fraction of AH production is by a secretory process that is independent of the pressure in the eye, the remainder of AH is produced by ultrafiltration [9]. If the trabecular meshwork is obstructed, or if a displaced iris prevents access to the trabecular meshwork, the intraocular pressure (IOP) increases due to sustained AH production, often causing glaucomatous damage to the optic nerve.

The contour of the iris and its position in relation to the other structures in the anterior chamber are significant in many forms of glaucoma [10]. Clinical observations of the iris contour changing after the iris is dilated [11] and after laser iridotomy (i.e., burning a small hole in the iris with a laser) [12] support the hypothesis that passive mechanical interaction of the AH with the

iris significantly influences the contour and position of the iris. In order to assess this hypothesis, one must determine whether the AH flow is sufficient to drive the observed changes in iris contour.

The small size of the anterior chamber, the low AH flow rate, and the difficulty in sampling inside the living eye impede experimental measurement of AH flow. Tracer substances have been used to measure the rate of AH flow, but these measurements are difficult to interpret for two reasons. First, the rate of AH production by the ciliary processes varies by a factor of two over a 12 hour period [13]. Second, diffusion contributes significantly to the total tracer flux in the anterior chamber (P cletnumber is order 1). Tracer methods have been shown to be effective in measuring the total rate of AH flow, but not valuable in determining the flow pattern of AH in the anterior segment [14].

The first hydrodynamic model of AH flow in the posterior and anterior chambers was developed by Friedland [4]. This model assumed that all the tissues in the eye were rigid and not affected by the flow of AH. The geometry of the eye was also simplified so that an analytical solution to the Stokes equations could be obtained in the anterior and posterior chambers (flow through the pupil was ignored). Tiedeman [3] solved for the contour of the iris by modeling it as a pressure relief valve. In the Tiedeman model, the edges of the iris were fixed, tension was placed on the iris at the inner radius, and there was uniform pressure acting on the lower surface. The Tiedeman model assumed that iris is infinitely thin and ignored the flow of AH.

We present herein a model that extends the previous work by accounting for the coupling between aqueous humor flow and passive deformation of a finite-thickness iris. This more complex model necessarily requires a more detailed physical description of the anterior eye, including aqueous humor and iris properties and specification of the various boundary conditions associated with healthy and diseased eyes.

Model Development

Aqueous humor has a density, ρ, of 1000 kg m^{-3} [15] and a viscosity, μ, of 7.5˚x˚10^{-4}˚kg m^{-1} s^{-1} at 37¡C [16]. A characteristic length scale for the flow of 5 x 10^{-4} m was chosen based on the height of the inlet used in the model, and the characteristic velocity of 2 x 10^{-6} m/sec was chosen based on the average velocity at the inlet. A representative Reynolds number of 0.001 is then calculated for the flow in the eye, consistent with Friedland's [4] earlier estimate and the neglect of inertia. The AH is therefore modeled using the transient Stokes flow equations:

$$\nabla \cdot \underline{v} = 0 \tag{1}$$

$$\rho \frac{d\underline{v}}{dt} = -\nabla P + \mu \nabla \cdot \left[\nabla \underline{v} + \left(\nabla \underline{v} \right)^{T} \right] \tag{2a}$$

$$\rho \frac{d\underline{v}}{dt} = -\nabla P + \mu \nabla^{2} \underline{v} \tag{2b}$$

where $\underline{v}$ is velocity and P is pressure. The form of Eq. (2a) is the form actually used to solve the problem because it allows natural incorporation of total normal stress boundary conditions [17]; Eq. (2b), the more commonly written form, is equivalent in the case of incompressible flow and is included for clarity. The transient term, $d\underline{v}/dt$, is included in the model even though the Reynolds number is small because some ocular events, such as blinking, happen on short time scales. Experiments on the bovine iris have shown that the tissue is incompressible and linearly elastic under small deformations with a Young's modulus, E, of 27 kPa in the radial direction [18]. These measurements support the use of the incompressible linear elastic equations to model the iris:

$$\nabla \cdot \underline{u} = 0 \tag{3}$$

$$-\nabla P + G\nabla \bullet \left[\nabla \underline{u} + \left(\nabla \underline{u} \right)^{T} \right] = 0 \tag{4a}$$

$$-\nabla P + G\nabla^{2} \underline{u} = 0 \tag{4b}$$

where $\underline{u}$ is displacement from the rest position, and Eqs. (4a) and (4b) are the solid analogs of Eqs. (2a) and (2b). A shear modulus, G, of 9 kPa is used in the model because the iris is incompressible (E=3·G). The rest position of the iris is assumed to be planar (Fig. 2) based on the observation of aphakic eyes. Although the supposed rest position of the iris is inside the lens, hydrodynamics of the aqueous humor force the iris away from the lens surface. The region of the eye being modeled is assumed to be axisymmetric, reducing Eqs. (1-4) to only 2 computational dimensions.

Boundary Conditions

The model domain is shown in Fig. 2. Most of the dimensions used in the model are based on the ultrasound biomicroscopy measurements of Fontana and Brubaker [8]. Additional dimensional information is based on the ultrasound biomicroscopy work of Thijssen [19] and Sokol *et al.* [20]. The boundary conditions used to describe the normal eye follow, along with modifications to account for variation in properties and for pathological cases.

Normal Eye

Both the trabecular meshwork and the vitreous gel are treated as rigid penetrable boundaries. Thus, the tangential velocity of AH at these boundaries is set to zero (no slip). The following equation gives the relation between the normal velocity and the pressure at the trabecular meshwork [21]:

$$v_{n} = \frac{C_{TM} \left(P_{Outlet} - P_{Vein} \right) + F_{u}}{A_{Outlet}} \tag{5}$$

where v_n is the normal velocity, P_{Outlet} is the pressure in the AH at the outlet, A_{Outlet} is the area of the trabecular meshwork, and μ is the viscosity of the AH. The venous pressure, P_{vein}, is estimated to be 1.2 kPa (9 mm Hg, [22]). The cross-sectional area of the trabecular meshwork, A_{Outlet}, is 18 mm^2 in the model. The hydraulic conductivity of the trabecular meshwork, C_{TM}, is set to 3.8 x 10^{-5} μL s^{-1} Pa^{-1} (0.3 μL min^{-1} mm Hg^{-1}) and the uveoscleral flow, F_u, is set to 6.7 x 10^{-3} μL s^{-1} (0.4 μl min^{-1}), typical values for the human eye [21].

A simplified version of Eq. (5) is used to set the velocity through the posterior outflow pathway.

$$v_n = \frac{C_{PP}\,(P_{Outlet} - P_{Vein})}{A_{Vit}} \tag{6}$$

The hydraulic conductivity of the posterior pathway, C_{PP}, includes the resistance of the vitreous, retina, retinal pigment epithelium, and sclera. There currently is little information on posterior flow in a normal eye, presumably due to the insignificance of the flow and the difficulty in measuring the flow due to active transport across the blood-retinal barrier [23]. Maurice [24] argued that based on movement of tracer from vitreous into the anterior chamber, the fluid in the vitreous body is approximately stagnant. Araie *et al*. [25] reported that systemic acetazolamide generated a small posterior flow through the vitreous equivalent to 1-2% of the total aqueous flow rate. Epstein *et al.* [26] injected fluorescein-containing solution into the anterior chamber and vitreous, and in neither case was their any flow from the optic nerve, vortex veins, or posterior sclera, indicating a low conductivity compared to the TM and anterior sclera. Based on these measurements, we have initially to set the hydraulic conductivity of the posterior pathway to zero. The sensitivity of the solution to other possible values for the hydraulic conductivity is also explored. The cross-sectional area of the vitreous-aqueous humor interface, $A_{vit,}$ is 65 mm^2.

The normal stress along the inlet is set to zero so that the pressure is properly scaled in the problem. The IOP in the eye is calculated by including the constraint that the inlet flow rate be equal to 2.5 μL/min (i.e, a constant inlet flow rate). In the human eye, the flow rate of AH is

reduced at elevated IOP by approximately 0.5% to 1% per mm Hg [27], but this effect is not included in the model. As the conductivities of the outflow pathways are changed, both the IOP and the corneal position change so that the aqueous humor can continue to flow into the eye at a constant rate, as has been observed clinically [28]. The IOP is largely determined by the permeability of the trabecular meshwork and the posterior pathway, but resistances to flow between the iris and lens as well as throughout the anterior eye are included in the calculation.

The cornea is extremely stiff, permitting it to be modeled as a shell. The edges of the cornea are assumed to be fixed at the periphery, so we neglect radial displacement of the cornea. Axial (i.e., anterior/posterior) displacement is calculated by approximating the cornea as a spherical elastic shell [29]:

$$P_{eye} = P_0 + \frac{2 \cdot E \cdot L_{cornea} \cdot u_z}{R^2_{cornea} \cdot (1 - \nu)} \tag{7}$$

where L_{cornea} is the thickness of the cornea, P_0 is the IOP at which the cornea is not displaced from the normal position (assumed to be 15 mm Hg) and R_{cornea} is the radius of curvature for the cornea. The Poisson's ration, ν, of the cornea is assumed to be 0.5 [30]. The Young's modulus, E, of the cornea is set to 10.3 MPa [31] causing the axial displacement, u_z, to be small for the problems of interest here. It is common to describe the stiffness of the cornea-sclera shell in terms of ocular rigidity, but the ocular rigidity reflects the stiffness of the weakest part of the cornea-sclera shell and for this reason we use Eq. (7) with the experimentally measured modulus for the cornea. For situations in which there are large deformations of the cornea, (e.g., radial keratotomy, LASIK) the biphasic and viscoelastic nature of the cornea are important, and Eq. (7) cannot be used as an approximation [32]. The sclera is not included in the model, but the cornea shell could be extended using the appropriate modulus and radius for the sclera.

The peripheral attachment of the iris is treated as fixed (i.e., no displacement). The displacement of the iris is calculated by setting the viscous traction in the fluid equal to the elastic traction exerted by the iris at the iris-AH interface. The velocity of the AH at the surface of the

iris is set equal to the velocity of the iris (i.e., no slip). Similarly, the velocity of AH along the surface of the lens is set equal to the velocity of the lens (normally zero). The lens capsule is quite stiff ($E \cong 20$ MPa, [33]), and the position and contour of the lens are generally controlled actively, so we treat the lens as uninfluenced by aqueous humor dynamics and prescribe its position/movement.

The zonules are the fibers connecting the lens to the ciliary body. Because of space between them, individual zonules cannot be included in our axisymmetric model. Resistance to flow caused by the zonules is lumped into the posterior flow permeability parameter, C_{PP}. The position of the zonules within the eye can be estimated from ultrasound biomicroscopy (e.g., Pavlin *et al.*, [34]), so the distance between the zonules and iris could be calculated.

Miosis

The pupil diameter can vary from 1 mm to 9 mm in the human eye [35]. The diameter in the model is normally 3 to 4 mm. Additional finite element meshes were created in which the pupil diameter was reduced to 1 mm and 2 mm and increased to 6 mm. For this work, we only solved steady state problems and did not consider the transient behavior during miosis/dilation. Even though the modulus of the iris may change during miosis, a shear modulus of 9 kPa is used for all pupil diameters due to the lack of experimental data available to quantify the change.

Blinking

The human blink lasts for approximately 200 ms [36]. Men blink approximately every 2.8 s, and women blink slightly less than every 4 s [37]. Blinking is modeled by applying a compressive normal stress along the cornea and trabecular mesh for the duration of a blinking. This is accomplished by adding a negative stress term to the left-hand side of Eq. (7). The magnitude of the normal stress is based on measurements of the intraocular pressure in rabbit eyes during a blink. Percicot *et al.* [38] measured a pressure increase of 2.0 kPa during a blink. Previously, Collins [39] measured pressure changes as high as 9.3 kPa in rabbit eyes but stated that these were extreme instances.

Iris Bomb

The model for the normal eye can be modified to represent various diseased conditions. For example, iris bomb occurs when an inflammatory membrane seals the iris to the lens near the pupil margin [40]. Since iris bomb clearly involves passive deformation of the iris, it was chosen as a test case for our simulation. In theory, the pressure in the posterior chamber could be very high (> 50 mm Hg) depending on the conductivity of the posterior pathway, and the pressure at the outlet could be as low as the venous pressure (1.2˚kPa or 9 mm Hg). However, it is unlikely that the pressure difference between chambers could ever be this great because that would require a perfect seal between the iris and lens. Our objective in modeling iris bomb is to estimate the pressure difference between the anterior and posterior chambers required to achieve the extreme anterior displacement visible in ultrasound biomicroscopy. There are a large number of unknowns involved in modeling this condition, including the change in outflow resistance due to the displaced iris, the conductivity of the posterior pathway (which becomes more important as the posterior chamber pressure increases), and the resistance to flow between the iris and lens. Rather than focus on those issues, which largely determine AH flow but not iris contour, we chose to test our model by concentrating on the iris contour, which depends almost exclusively on the pressure difference between the posterior and anterior chambers.

To model iris bomb, the iris tip is fixed in place next to the lens. Since the displacement of the iris is almost entirely determined by the hydrostatic pressure differences between the chambers, the AH flow is set to zero between the iris and lens to simplify the problem. The pressure at the inlet is set to zero for scaling purposes, and the pressure at the outlet is varied until the desired iris curvature is achieved. The fixed pupil margin and eliminated AH flow essentially reduce our model to Tiedeman's model (except that our model uses a finite-thickness iris).

Numerical Solution

Finite element meshes (e.g., Fig. 3) are generated using the FIGEN module of the FIDAP finite element package (Fluent Incorporated; Lebanon, NH). Meshes containing between 200 and 500 elements are normally used in the model. Because of the free-surface problem associated with the iris-aqueous interface, the AH domain is not known *a priori*. We therefore guess the iris position and generate an initial mesh of the aqueous domain based on that iris position. As the iris position is updated, the AH domain and its associated mesh are updated by the pseudo-solid method [41]. A compressible elastic solid equation is solved on the AH domain, and the mesh points are moved with the deformation of the pseudo-solid.

The finite element discretization of the model equations is accomplished by a mixed formulation. The velocity of the AH, the displacement of the iris, and the displacement of the pseudo-solid are described by piecewise biquadratic basis functions; the pressure is described by piecewise linear basis functions. The linear problem associated with each Newton step is solved iteratively using the incomplete-LU-preconditioned GMRES method [42].

Transient phenomena (such as blinking) are modeled using the implicit Euler method. Thus, the no-slip condition between the AH and a moving tissue is given by:

$$v_{AH}(t) = \frac{u_{tissue}(t) - u_{tissue}(t - \Delta t)}{\Delta t} \tag{8}$$

The time step used depended on the time scale of the phenomena under study. In general, we found that a time step of 10% of the characteristic time scale was sufficient (i.e., the simulation results did not change significantly with temporal refinement). For blinking, which occurs over tenths of a second, $\Delta t = 0.01$ s was used.

Results

Normal Eye

An ultrasound biomicrograph of the peripheral iris [43] for a healthy eye (Fig. 4a) shows clearly the angle between the iris and cornea in a healthy eye. Figure 4b is an ultrasound taken

at an off-axis angle, which shows the proximity of the iris to the lens near the pupil. The resolution of an ultrasound biomicrograph (c. 50 μm, [44]) is not sufficient to resolve the space between the iris and the lens. Since the AH flows between the iris and lens, they cannot be completely in contact, but the distance is less than 50˚μm based on the ultrasound measurements.

The corresponding model result for a healthy eye based on the boundary conditions given above is shown in Fig. 5, with the flow pattern through the pinch between the iris and the lens included as an enlargement.

Marchini *et al.* (1998) defined the apparent iris-lens contact distance to be the radial distance from the pupil margin to the point at which separation between the iris and the lens was detectable with ultrasound biomicroscopy. They reported an apparent iris-lens contact distance of 0.66 – 0.10 mm (mean – standard deviation, n = 42) with an estimated 50 μm resolution limit for the ultrasound. In a similar study by Liebmann *et al.* [45], the initial ultrasound images showed 0.77 – 0.10 mm of apparent iris-lens contact; after a 15 minutes of continuous measurements, the apparent contact distance had reduced to 0.55 – 0.09 mm. The model predicts that the iris-lens gap is less than 50 μm for a distance of 0.60˚mm, consistent with the measurements of Marchini and Liebmann.

The maximum velocity of aqueous humor is 1.01 mm/s, which is about 3 orders of magnitude higher than the velocity in the anterior and posterior chambers. Although the velocity is relatively high in the pinch, the small length scale limits the maximum value of the Reynolds number to 0.004, so inertia is still negligible. The IOP in the model solution is 2.1 kPa (16 mm Hg) for an AH flow rate of 2.5˚μL/min and an iris shear modulus of 9 kPa. Clinical measurements of the IOP in healthy eyes are typically 1.7 to 2.3 kPa (13 to 17 mm Hg) [46]. The pressure drop between the anterior and posterior chambers is 31.2 Pa (0.23 mm Hg), negligibly small compared to IOP.

Many of the parameters in the model were estimated from incomplete or circumstantial data, so we explored the model sensitivity over a reasonable range of values. Well-established

parameters (e.g., aqueous humor viscosity) were not included in the sensitivity analysis. Specifically (see Table 1), trabecular permeability, posterior pathway permeability, iris stiffness, and aqueous humor flow rate were varied.

Miosis

Increasing the pupil diameter has little effect on the results since the thicker iris (N.B., the iris is incompressible) is less flexible, and the iris is further from the lens. The effect of constricting the pupil to 2 mm, however, is more significant, as seen in Fig. 6. The pressure drop between the anterior and posterior chamber is increased to 50.5 Pa (0.38 mm Hg), and the iris contour becomes more convex. The minimum iris-lens distance is 4.8˚μm, and the iris-lens gap is less than 50 μm for a distance of 0.69 mm. The effects of miosis are even more dramatic when the pupil diameter is decreased to 1 mm. The pressure difference between the chambers becomes 58.9 Pa (0.39 mm Hg), and the minimum iris-lens distance is increased to 8.4 μm. The apparent iris-lens contact length in increased to 1.13 mm, and the maximum velocity in the eye reaches 2.2 mm/sec.

The model predicts an increase in the apparent iris-lens contact as the pupil diameter decreases. At a pupil diameter of 6 mm, for example, the model predicts only 0.38 mm of apparent iris-lens contact, but at a diameter of 2 mm, the distance is reduced to 0.69 mm. Woo et al. [47] measured the apparent contact distance under light and dark conditions in eyes with pupillary block. In dark conditions, the distance was 0.350 ± 0.020 mm, and in the light, the distance was increased to 0.693 ± 0.035 mm.

Blinking

The predicted IOP during blinking is shown in Fig. 7. When the normal stress caused by the eyelid is removed immediately after blinking, the IOP experiences a minimum due to the forward movement of the cornea. The IOP increases until the inlet and outlet flow rates are again equal. The maximum velocity of the fluid near the cornea during a blink is approximately 1˚x 10^{-7} m/s, so the assumption of transient Stokes flow remains valid.

Iris Bomb

Iris Bomb results in an extreme anterior bulging of the iris, which can be observed clearly using ultrasound biomicroscopy (Fig. 8a, from [40]), and a corresponding rise in IOP. We found that a 1.3 to 2.0 kPa (10 to 15 mm Hg) pressure difference between chambers (corresponding to severe but not total pupillary block —see Discussion) captured the basic contour of iris bomb . The iris contour predicted by the model (Fig. 8b) is very similar to that shown in the ultrasound taken of a patient with iris bomb . The pressure difference between the chambers in Fig. 8b is 1.7 kPa (12.8 mm Hg). Pressure differences higher than 2.0 kPa (15 mm Hg) led to contact between the anterior surface of the iris and the posterior surface of the cornea, as is seen in the ultrasound biomicrograph in Fig. 8a [40]. Our current model is unable to account for such severe angle closure for two reasons. First, it may occur in only a portion of the iris, thus being beyond the scope of our axisymmetric model. Second, our computer program is not equipped to solve a contact problem, and instead the program fails when it tries to place the iris within the cornea.

Discussion

The difficulties associated with experimentally determining the flow pattern of the AH are well documented (e.g., [13]). We have developed a mathematical model of the anterior segment that enables theoretical investigation of the passive mechanical interaction between AH and iris. Simulation of a normal eye shows the iris being displaced by the AH as it circulates through the anterior segment. The model predictions of iris contour and apparent iris-lens contact distance agree well with published ultrasound biomicroscopy results. The iris displacement is primarily a function of the aqueous flow rate, trabecular meshwork permeability, the permeability of the posterior pathway, and iris modulus. As Table 1 demonstrates, the model results change in a logical way when these parameters are varied.

Blinking is modeled by applying a normal stress along the cornea. Because the model is axisymmetric, the eyelid can only be modeled in the completely open or completely closed state.

As a result, the model prediction for the magnitude of the rise in IOP during blinking agrees well with measurements on the rabbit eye - in essence it must because the normal stress sets the IOP - but the shape of the pressure curve has poor agreement. The experimental pressure curve gradually approaches a maximum as the eye lid is closing, but the theoretical pressure curve from the model almost immediately reaches a maximum because the closing of the lid occurs in a single time step. While it may be possible to correct this discrepancy by including a smoother pressure vs. time profile, a more accurate approach would be to relax the assumption of axisymmetry, which is important for other reasons discussed below. Published measurements of IOP during blinking [38, 39] include a pressure minimum 0.2 to 0.3 kPa below normal immediately following the blink. This is 100 times larger than the 2 Pa drop predicted by the model. Possible explanations for this discrepancy include the location of the pressure transducer in the vitreous, the absence of the sclera in the model, noise due to the rapid pressure fluctuations, and the smaller ocular volume in rabbit leading to greater sensitivity to corneal motion.

The model allows exploration of AH-iris interactions in iris bomb . The pressure difference between the anterior and posterior chambers in eyes with iris bomb has not been previously measured, but estimates are possible using the model described here. The smallest possible pressure difference necessary to achieve the dramatic iris contour observed in ultrasound images is 1 kPa (7.5 mm Hg). The pressure difference in the normal eye is 31 Pa according to the model. The 30-fold increase in pressure difference corresponds to a 97% reduction in facility through the pupil margin. Since flow rate through a narrow slit goes as the cube of the slit width, even a relatively small amount of contact could cause the dramatic drop in facility. If, for example, 10% of the iris at the pupil margin were actually attached to the lens, and the other 90% were held so that the gap width between iris and pupil dropped by a factor of 3 from the normal case, the result would be a 30-fold increase in the pressure difference between the anterior and posterior chamber. Of course, such an effect would not be

axisymmetric (since the iris would be attached at some points and not others, but our simplified model does allow us to consider iris bomb in a spatially-averaged sense.

The results of Figures 5 and 6 allow us to compare our model with the previous work of Tiedeman [3]. We first assess whether our inclusion of shear stress and non-uniform pressure within the chambers (neglected by Tiedeman) has a significant effect on iris contour. As can be seen in Figures 5 and 6, the pressure is essentially uniform in each chamber, validating Tiedeman assumption. From the expanded view of the pinch in Figure 5, we can estimate a maximum shear rate of (1 mm/s) / (10 m) = 100 s^{-1}, whichfor aqueous humor corresponds to a shear stress of approximately 0.1 Pa. Since the pressure drop between the chambers is on the order of 30 Pa (Table 1), we conclude that, at least under normal conditions, shear stress from the aqueous has a negligible effect on iris contour.

We observe, however, that Tiedeman s model did not account for finite thickness of the iris, nor for the coupling between the aqueous humor flow and the pressure difference between the chambers. Since Tiedeman s model required specification of the pressure difference and of the point of contact between iris and lens, the effect of, for example, changes in AH flow rate could not be calculated directly. One might incorrectly assume (following Friedland [4]) that the gap between the iris and the lens does not change significantly, which would imply (because of the linearity of the fluids problem) that the pressure difference between the chambers is proportional to the AH flow rate. In fact (Table 1), the pressure difference is virtually constant for flow rates between 1.5 and 3.5 µL/min because the larger flow rate is accommodated by increasing iris-lens gap. The Tiedeman model requires specification of the nominal iris-lens attachment point, making predictive analysis difficult. The Tiedeman model is ideally suited for the evaluation of a clinically measured iris contour, for which one could very quickly determine (1) what the pressure difference between the posterior and anterior chambers is, and (2) whether the iris is in fact behaving as a uniform sheet or whether there are other complicating mechanical features (e.g., a tumor or severe scar). Our model has greater flexibility (with the corresponding complexity) and is thus more suited to simulation and prediction.

The model predictions of iris contour and IOP in normal eyes are consistent with clinical observation. In some cases, specific model parameters are responsible for the agreement, such as the IOP in the normal eye being sensitive to AH flow rate and trabecular permeability but little else. Iris-lens distance in healthy eyes is too small to measure accurately with current experimental technology, so it forms an imperfect test of the model. However, model predictions of apparent iris-lens contact distance are in good quantitative agreement with ultrasound measurements. The change in apparent contact with different pupil diameters is also in good agreement with experimental results. While this test is imperfect because the experimental measurements were made on eyes with pupillary block, the qualitative agreement is encouraging. In the future, we hope to examine demographic variations in domain geometry, which are correlated with demographic risk factors for different types of glaucoma [1].

A major simplification made in this analysis is that the eye is axisymmetric. The eye is nearly symmetric about the center axis, although it does have a slight asymmetry due to the location of the pupil [35]. The zonules break the symmetry of the eye, but they are approximated as a thin, permeable sheet instead of individual fibers. In addition, the characteristic shape and alignment of the Krukenberg spindle in pigmentary glaucoma patients suggests a non-axisymmetric flow pattern in the aqueous [2], possibly due to free convection caused by the aqueous being cooler (and thus denser) near the cornea than near the iris. The density gradients arising from free convection are small and would have little influence on the passive iris position. We doubt that these breaks in symmetry significantly affect the contour of the iris, but they are clearly important in the understanding of the hydrodynamics of aqueous humor.

Peripheral laser iridotomy (PI), in which small holes are burned through the iris, has been used to treat pigmentary [12] and acute angle closure glaucoma [48]. The iridotomy breaks the natural symmetry of the iris, so a fully three-dimensional model will be necessary to simulate this treatment. Since the primary effect of PI is to reduce transiridal pressure drop, the treatment will be an excellent subject for our model once we have extended to three dimensions. The

development of a 3-dimensional model is possible, in part, because of the ability to obtain 3-dimensional ultrasounds of the eye [49].

The other major limitation of the model is that it includes only a portion of the eye. As a result, it is unable to account for many phenomena that are important in ophthalmic health and disease. Aqueous misdirection, for example, involves significant changes in the posterior eye. Perhaps more broadly important is the relationship between the position of the peripheral iris, which our model assumes fixed) and outflow facility. A larger model, incorporating a larger portion of the eye, would allow us to explore the mechanical interrelations between ocular components more thoroughly and would provide greater insight into the mechanisms of glaucoma and how to treat them. Although formulation, solution, and experimental specification of such a model would all be considerable tasks, the potential advantages are sufficient to make them worth pursuing. We see the model in this paper as a smallestsignificant domain model, encompassing enough of the eye to allow for simulation of some phenomena but limited to a small enough region to allow solution of the model equations.

Acknowledgments

We thank Joel S. Schuman, Charles J. Pavlin, Kasia Harasiewicz, and F. Stuart Foster for graciously providing the ultrasound biomicrographs included in this paper. This work was supported by a Whitaker Foundation Bioengineering Research Grant and by National Eye Institute grant R01-EY12291-01; simulations were possible through the support of University of Minnesota Supercomputing Institute for Digital Simulation and Advanced Computation.

References

1. Quigley, H. A., 1996, Number of People with Glaucoma Worldwide, British Journal of Opthalmology, **80**, pp. 389-393.
2. Farrar, S. M. and Shields, M. B., 1993, Current Concepts in Pigmentary Glaucoma, Survey of Ophthalmology, **37**, pp. 233-252.
3. Tiedeman, J. S., 1991, A Physical Analysis of the Factors That Determine the Contour of the Iris, American Journal of Ophthalmology, **111**, pp. 338-343.
4. Friedland, A. B., 1978, A Hydrodynamic Model of Aqueous Flow in the Posterior Chamber of the Eye, Bulletin of Mathematical Biology, **40**, pp. 223-235.
5. Van Buskirk, E. M., 1997, "Anatomy," Chandler and Grant's Glaucoma, Epstein, D. L., *et al.*, eds., Williams & Wilkins, Baltimore, pp. 6-17.
6. Fatt, I., 1975, Flow and Diffusion in the Vitreous Body of the Eye, B Math Biol, **37**, pp. 85-90.
7. Caprioli, J., 1992, "The Ciliary Epithelia and Aqueous Humor," *Adler's Physiology of the Eye : Clinical Application*, Hart, W. M., ed., Mosby-Year Book, St. Louis, pp. 228-247.
8. Fontana, S. T. and Brubaker, R. F., 1980, Volume and Depth of the Anterior Chamber of the Normal Aging Human Eye, Archives of Ophthalmology, **98**, pp. 1803-1808.
9. Bartels, S. P., 1989, "Aqueous Humor Formation. Fluid Production by a Sodium Pump," *The Glaucomas*, Ritch, R., *et al.*, eds., C.V. Mosby Company, St. Louis, Vol 1, pp. 199-218.
10. Liebmann, J. M. and Ritch, R., 1996, Ultrasound Biomicroscopy of the Anterior Segment, Journal of the American Optometric Association, **67**, pp. 469-479.
11. Pavlin, C. J., Harasiewicz, K., and Foster, F. S., 1995, An Ultrasound Biomicroscopic Dark-Room Provocative Test, Ophthalmic Surgery, **26**, pp. 253-255.
12. Karickhoff, J. R., 1992, Pigmentary Dispersion Syndrome and Pigmentary Glaucoma: A New Mechanism Concept, A New Treatment, and A New Technique, Ophthalmic Surgery, **23**, pp. 269-277.
13. Smith, S. D., 1991, Measurement of the Rate of Aqueous Humor Flow, The Yale Journal of Biology and Medicine, **64**, pp. 89-102.
14. Mclaren, J. W., Ziai, N., and Brubaker, R. F., 1993, A simple three-compartment model of anterior segment kinetics, Exp. Eye Res., **56**, pp. 355-366.
15. Scott, J. A., 1988, A Finite Element Model of Heat Transport in the Human Eye, Phys. Med. Biol., **33**, pp. 227-241.
16. Beswick, J. A. and McCulloch, C., 1956, Effect of Hyaluronidase on the Viscosity of the Aqueous Humour, Brit. J. Ophthal., **40**, pp. 545-548.
17. Gunzburger, M. D., 1989, *Finite Element Methods for Viscous Incompressible Flows: A Guide to Theory, Practice, and Algorithms*, Academic Press, Boston.
18. Heys, J. and Barocas, V. H., 1999, Mechanical Characterization of the Bovine Iris, Journal of Biomechanics, **32**, pp. 999-1003.

19. Thijssen, J. M., 1993, The History of Ultrasound Techniques in Ophthalmology, Ultrasound in Med. & Biol., **19**, pp. 599-618.
20. Sokol, J., Stegman, Z., Liebmann, J. M., and Ritch, R., 1996, Location of the Iris Insertion in Pigment Dispersion Syndrome, Ophthalmology, **103**, pp. 289-293.
21. Kaufman, P. L., 1989, "Pressure-dependent Outflow," The Glaucomas, Ritch, R., *et al.*, eds., C.V. Mosby Company, St. Louis, Vol 1, pp. 219-240.
22. Johnson, M. C. and Kamm, R. D., 1983, The Role of Schlemm's Canal in Aqueous Outflow from the Human Eye, Invest Ophthalmol Vis Sci, **24**, pp. 320-325.
23. Cantrill, H. L. and Pederson, J. E., 1984, Experimental Retinal Detachment VI. The Permeability of the Blood-Retinal Barrier, Arch Ophthalmol, **102**, pp. 747-751.
24. Maurice, D. M., 1987, Flow of water between aqueous and vitreous compartments in the rabbit eye, Am. J. Physiol., **252**, pp. F104-F108.
25. Araie, M., Sugiura, Y., Sakurai, M., and Oshika, T., 1991, Effect of Systemic Acetazolamide on the Fluid Movement Across the Aqueous-vitreous Interface, Exp. Eye Res., **53**, pp. 285-293.
26. Epstein, D. L., Hashimoto, J. M., Anderson, P. J., and Grant, W. M., 1979, Experimental perfusions through the anterior and vitreous chamber with possible relationships to malignant glaucoma, American Jouranl of Ophthalmology, **88**, pp. 1078-1086.
27. Johnson, M. and Erickson, K., 2000, "Mechanisms and Routes of Aqueous Humor Drainage," *Glaucoma*, Albert, D. M., *et al.*, eds., WB Saunders Co., Philadelphia, Vol 4, pp. 2577-2594.
28. Brown, J. D. and Brubaker, R. F., 1989, A Study of the Relation Between Intraocular Pressure and Aqueous Humor Flow in the Pigment Dispersion Syndrome, Opthalmology, **96**, pp. 1468-1470.
29. Roark, R. J., 1965, *Formulas for Stress and Strain*, McGraw-Hill, New York.
30. Puslow, P. P. and Karwatowski, W. S. S., 1996, Ocular Elasticity, Ophthalmology, **103**, pp. 1686-1692.
31. Smolek, M. K., 1994, Holographic Interferometry of Intact and Radially Incised Human Eye-bank Corneas, Journal of Cataract and Refractive Surgery, **20**, pp. 277-286.
32. Bryant, M. R. and McDonnell, P. J., 1996, Constitutive Laws for Biomechanical Modeling of Refractive Surgery, Journal of Biomechanical Engineering, **118**, pp. 473-481.
33. Krag, S., Olsen, T., and Andreassen, T. T., 1997, Biomechanical Characteristics of the Human Anterior Lens Capsule in Relation to Age, Investigative Ophthalmology & Visual Science, **38**, pp. 357-363.
34. Pavlin, C. J., Buys, Y. M., and Pathmanathan, T., 1998, Imaging Zonular Abnormalitites Using Ultrasound Biomicroscopy, Arch Ophthalmol, **116**, pp. 854-857.
35. Thompson, H. S., 1992, "The Pupil," Adler's Physiology of the Eye: Clinical Application, Hart, W. M., ed., Mosby Year Book, St. Louis, Missouri, pp. 412-441.
36. Ren, H. and Wilson, G., 1997, The Effect of a Shear Force on the Cell Shedding Rate of the Corneal Epithelium, Acta Ophthalmologica Scandinavica, **75**, pp. 383-387.

37. Hart, W. M., 1992, "The Eyelids," Adler's Physiology of the Eye: Clinical Application, Hart, W. M., ed., Mosby-Year Book, St. Louis, pp. 1-17.

38. Percicot, C. L., Schnell, C. R., Debon, C., and Hariton, C., 1996, Continuous Intraocular Pressure Measurement by Telemetry in Alpha-Chymotrypsin-Induced Glaucoma Model in the Rabbit: Effects of Timolol, Dorzolamide, and Epinephrine, Journal of Pharmacological and Toxicological Methods, **36**, pp. 223-228.

39. Collins, C. C., 1967, Miniature Passive Pressure Transensor for Implanting in the Eye, IEEE Transactions on Bio-Medical Engineering, **14**, pp. 74-83.

40. Allingham, R. R., 1997, "Glaucoma Due to Intraocular Inflammation," *Chandler and Grant's Glaucoma*, Epstein, D. L., *et al.*, eds., Williams & Wilkins, Baltimore, pp. 375-394.

41. Sackinger, P. A., Schunk, P. R., and Rao, R. R., 1996, A Newton-Raphson Pseudo-Solid Domain Mapping Technique for Free and Moving Boundary Problems: A Finite Element Implementation, Journal of Computational Physics, **125**, pp. 83-103.

42. Saad, Y. and Schultz, M. H., 1986, GMRES: A Generalized Minimum Residual Algorithm For Solving Nonsymmetric Linear Systems, SIAM J Sci Stat Comp, **7**, pp. 856-869.

43. Pavlin, C. J. and Foster, F. S., 1998, Ultrasound Biomicroscopy: High-Frequency Ultrasound Imaging of the Eye at Microscopic Resolution, Radiologic Clinics of North America, **36**, pp. 1047-1058.

44. Marchini, G., Pagliarusco, A., Toscano, A., Tosi, R., Brunelli, C., and Bonomi, L., 1998, Ultrasound Biomicroscopic and Conventional Ultrasonographic Study of Ocular Dimensions in Primary Angle-closure Glaucoma, Ophthalmology, **105**, pp. 2091-2098.

45. Liebmann, J., Tello, C., Chew, S., Cohen, H., and Ritch, R., 1995, Prevention of Blinking Alters Iris Configuration in Pigment Dispersion Syndrome and in Normal Eyes., Ophthalmology, **102**, pp. 446-455.

46. Epstein, D. L., 1997, "Practical Aqueous Humor Dynamics," *Chandler and Grant's Glaucoma*, Epstein, D. L., *et al.*, eds., Williams & Wilkins, Baltimore, Maryland, pp. 18-24.

47. Woo, E. K., Pavlin, C. J., Slomovic, A., Taback, N., and Buys, Y. M., 1999, Ultrasound biomicroscopic quantitative analysis of light-dark changes associated with pupillary block, American Journal of Ophthalmology, **127**, pp. 43-47.

48. Liebmann, J. M. and Ritch, R., 1996, Laser Iridotomy, Ophthalmic Surgery and Lasers, **27**, pp. 209-221.

49. Downey, D. B., Nicolle, D. A., Levin, M. F., and Fenster, A., 1996, Three-Dimensional Ultrasound Imaging of the Eye, Eye, **10**, pp. 75-81.

Figure Captions

Fig. 1 Cross-section of the anterior segment of the eye showing the path of AH. The AH is secreted by the ciliary body and exits the eye through the trabecular meshwork. The posterior chamber is between the iris and lens, and the anterior chamber is between the cornea and iris.

Fig. 2 The model domain including the structure that each boundary represents and the iris in the rest position. The fluid domain is shown in gray, and the elastic solid domain is black.

Fig. 3 A typical mesh used in the model with 250 elements that results in approximately 4000 degrees of freedom. The mesh is highly refined in the pinch region between the iris and lens. The mesh is deformed slightly due to the movement of the iris.

Fig. 4 (a) An ultrasound biomicrograph of the peripheral iris of a healthy eye, and (b) an ultrasound biomicrograph of the iris taken from an off-axis angle to allow the spatial relationship between iris tip and lens to be shown. Visible in the ultrasounds are the cornea (C), iris (I), and lens (L). In (b), the iris is in apparent contact with the lens due to the ~50 μm resolution limit of the instrument. (Biomicrograph courtesy of CJ Pavlin, K Harasiewicz and FS Foster)

Fig. 5 The model prediction for the iris contour and flow profile for a healthy eye using normal boundary conditions. The velocity in the pinch region is approximately 3 orders of magnitude higher than elsewhere in the eye.

Fig. 6 A flow profile with the pupil diameter reduced to 2 mm. The iris now has a more convex contour and the pressure drop between the anterior and posterior chambers is doubled.

Fig. 7 The model prediction of IOP in a normal eye during blinking with every third time step shown. The blinking rate is set for every 2.8 sec., typical for males. The inset shows that there is a small, steady pressure rise between blinks.

Fig. 8 Iris bomb is a condition in which an inflammatory membrane seals the iris to the lens. (a) The extreme anterior bowing of the iris can be observed using ultrasound biomicroscopy. (b) This same behavior can be modeled by attaching the iris to the lens. The pressure difference between the anterior and posterior chamber is 1.7 kPa (13 mm Hg). Simulations were run with no AH flow for simplicity. (Biomicrograph courtesy of JS Schuman)

Table 1. Sensitivity of the model to selected parameters.

	Minimum iris-lens distance (μm)	ΔP between chambers (Pa, mm Hg)	IOP (kPa, mm Hg)	Maximum velocity (mm/s)	Apparent contact (mm)
Normal Eye C_{TM} = 3.8 x 10^{-5} μL s^{-1} Pa^{-1} C_{VP} = 0.0 μL s^{-1} Pa^{-1} G = 9 kPa Aqueous flow = 2.5 μL/min	4.4	31.2 (0.23)	2.1 (16)	1.01	0.60
C_{TM} = 3.0 x 10^{-5} μL s^{-1} Pa^{-1}	4.4	31.2 (0.23)	2.4 (18)	1.01	0.60
C_{TM} = 4.7 x 10^{-5} μL s^{-1} Pa^{-1}	4.4	31.2 (0.23)	1.9 (14)	1.01	0.60
C_{PP} = 6.5 x 10^{-7} μL s^{-1} Pa^{-1} ~2% of total flow is posterior	4.4	31.2 (0.23)	2.1 (16)	1.00	0.60
C_{PP} = 3.3 x 10^{-7} μL s^{-1} Pa^{-1} ~8% of total flow is posterior	4.3	31.2 (0.23)	2.1 (16)	0.97	0.60
C_{PP} = 6.5 x 10^{-6} μL s^{-1} Pa^{-1} ~15% of total flow is posterior	4.1	31.1 (0.23)	2.0 (15)	0.93	0.60
G = 20 kPa	3.0	68.7 (0.52)	2.1 (16)	1.33	0.63
G = 10 kPa	4.2	34.6 (0.26)	2.1 (16)	1.05	0.60
G = 8.1 kPa	4.6	28.1 (0.21)	2.1 (16)	0.97	0.60
G = 4.5 kPa	6.0	15.7 (0.12)	2.1 (16)	0.78	0.59
Aqueous flow = 1.5 μL/min	3.5	31.0 (0.23)	1.7 (13)	0.73	0.63
Aqueous flow = 2.0 μL/min	4.0	31.1 (0.23)	1.9 (14)	0.88	0.60
Aqueous flow = 3.0 μL/min	4.8	31.2 (0.23)	2.3 (17)	1.13	0.60
Aqueous flow = 3.5 μL/min	5.1	31.3 (0.23)	2.6 (20)	1.25	0.60

TM = trabecular meshwork
PP = posterior pathway

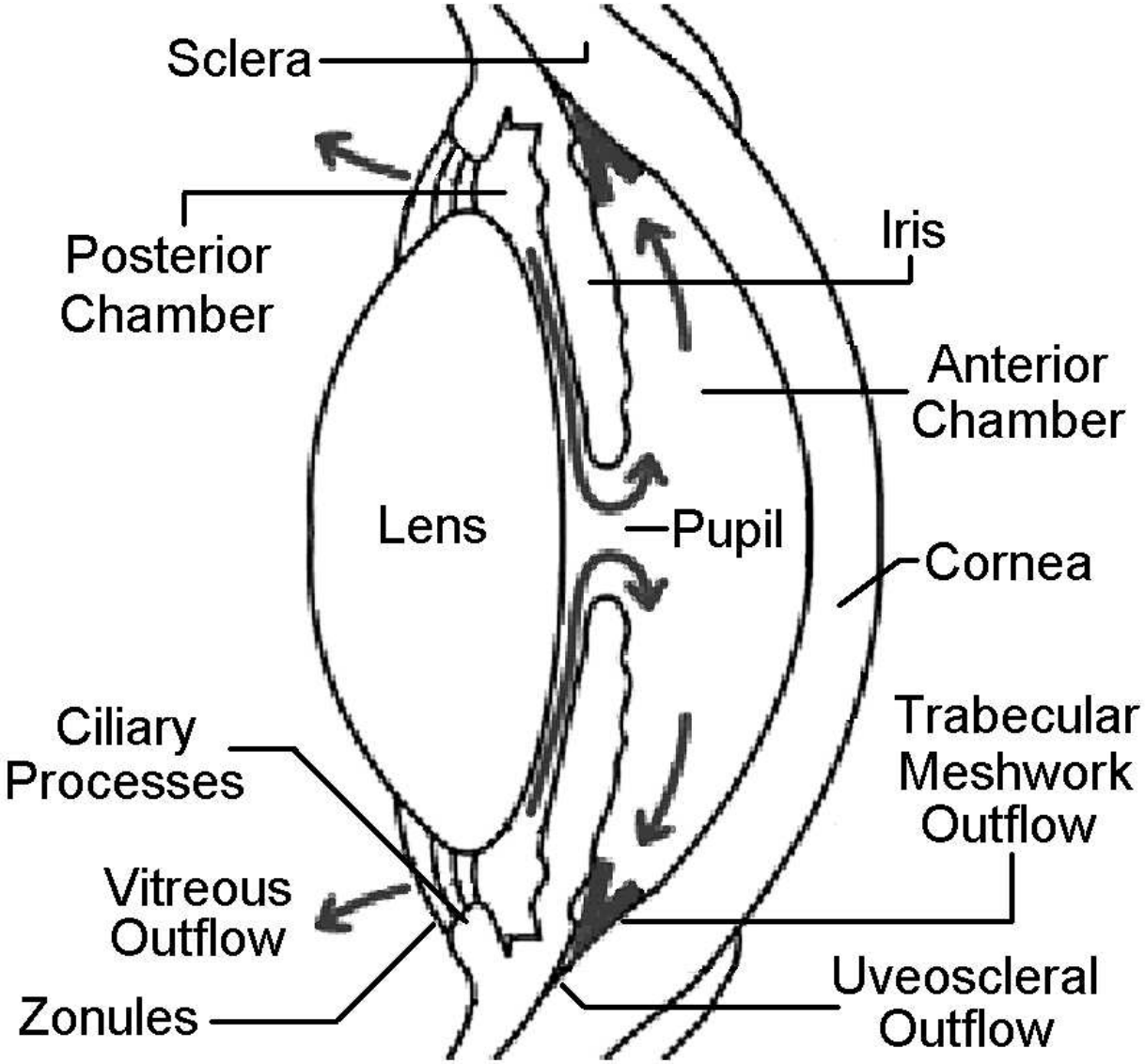
Sclera
Posterior Chamber
Iris
Anterior Chamber
Lens
Pupil
Cornea
Ciliary Processes
Trabecular Meshwork Outflow
Vitreous Outflow
Zonules
Uveoscleral Outflow

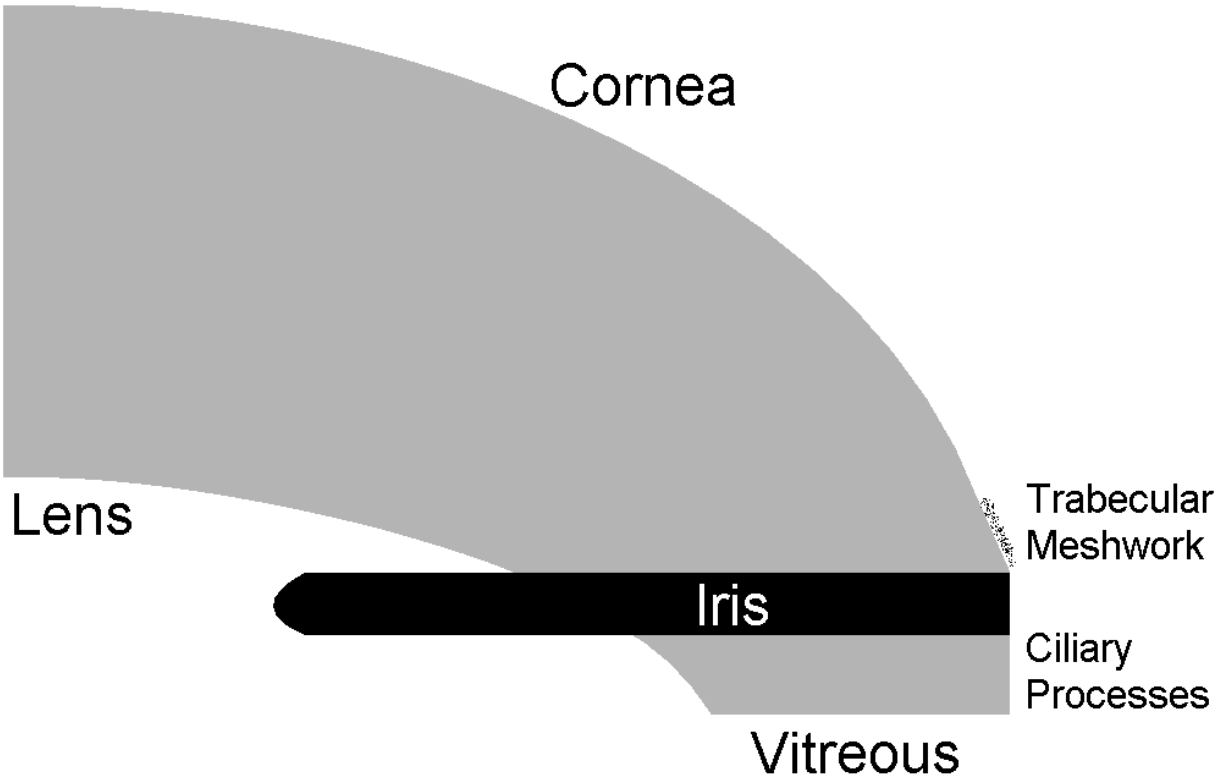
Cornea
Lens
Trabecular
Meshwork
Iris
Ciliary
Processes
Vitreous

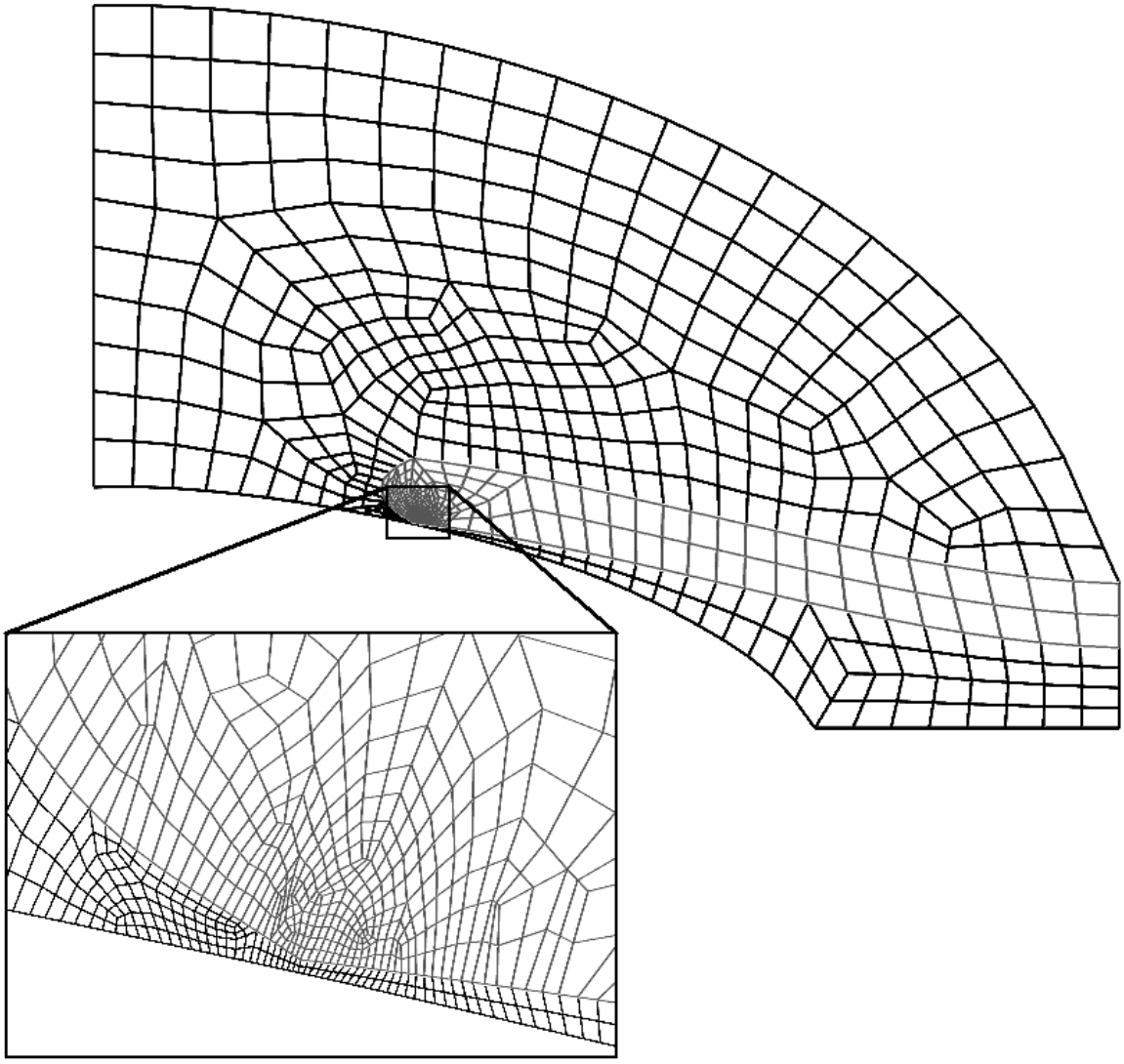

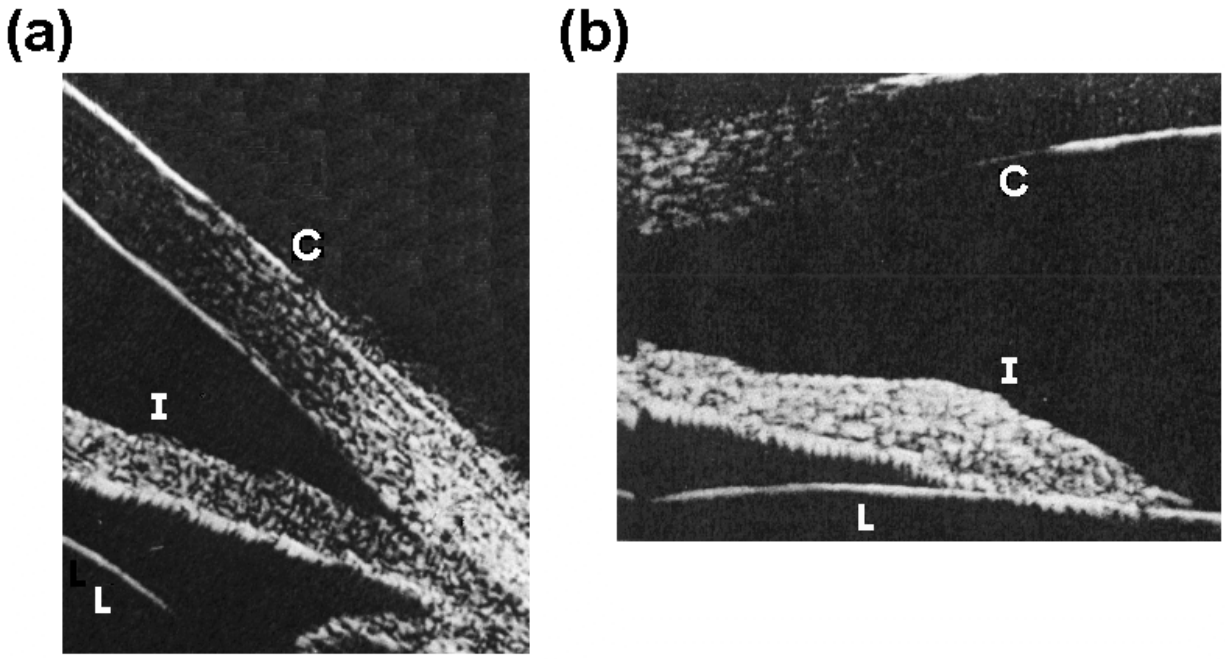
(a)
C
I
L
L
(b)
C
I
L

5

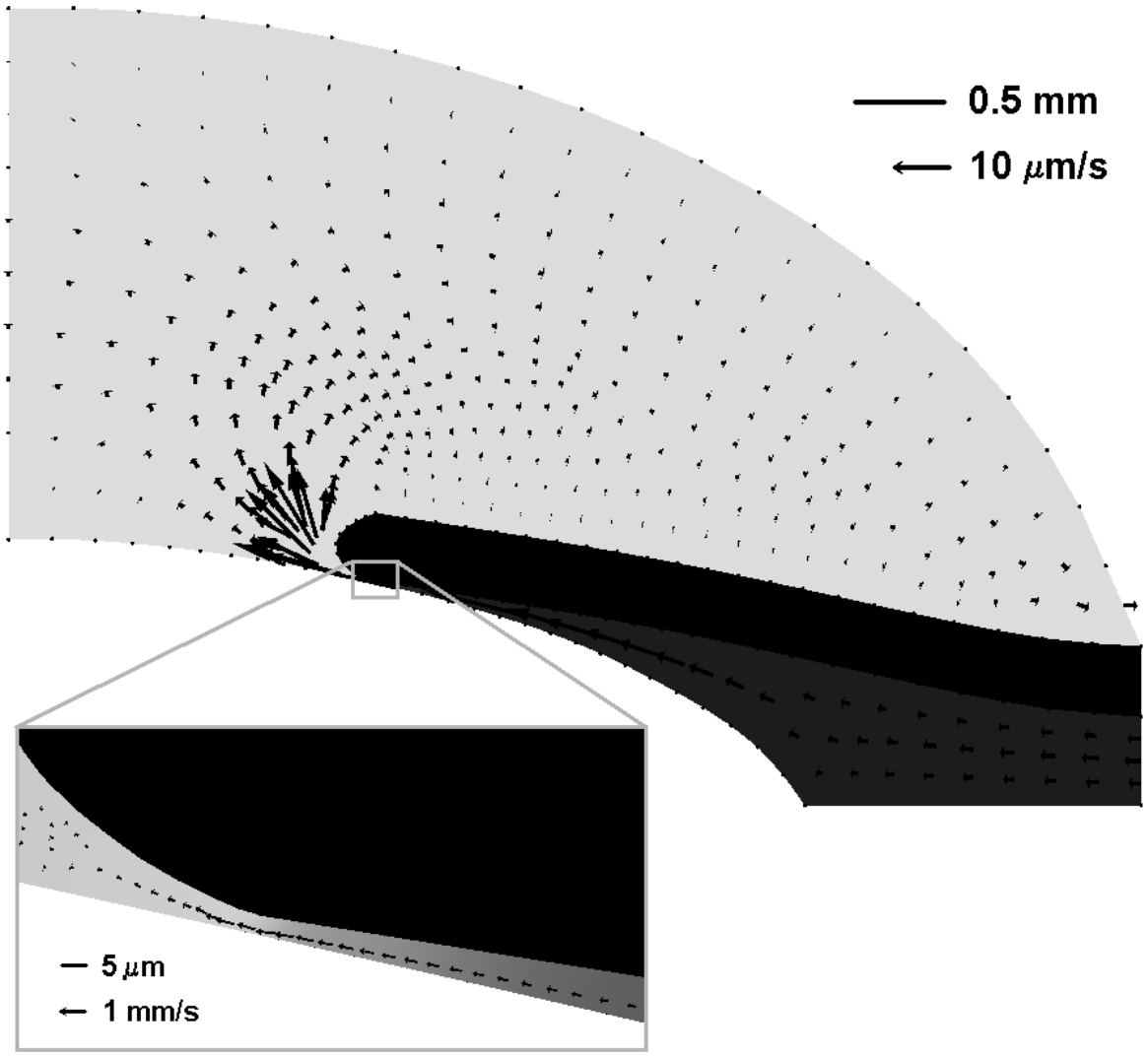

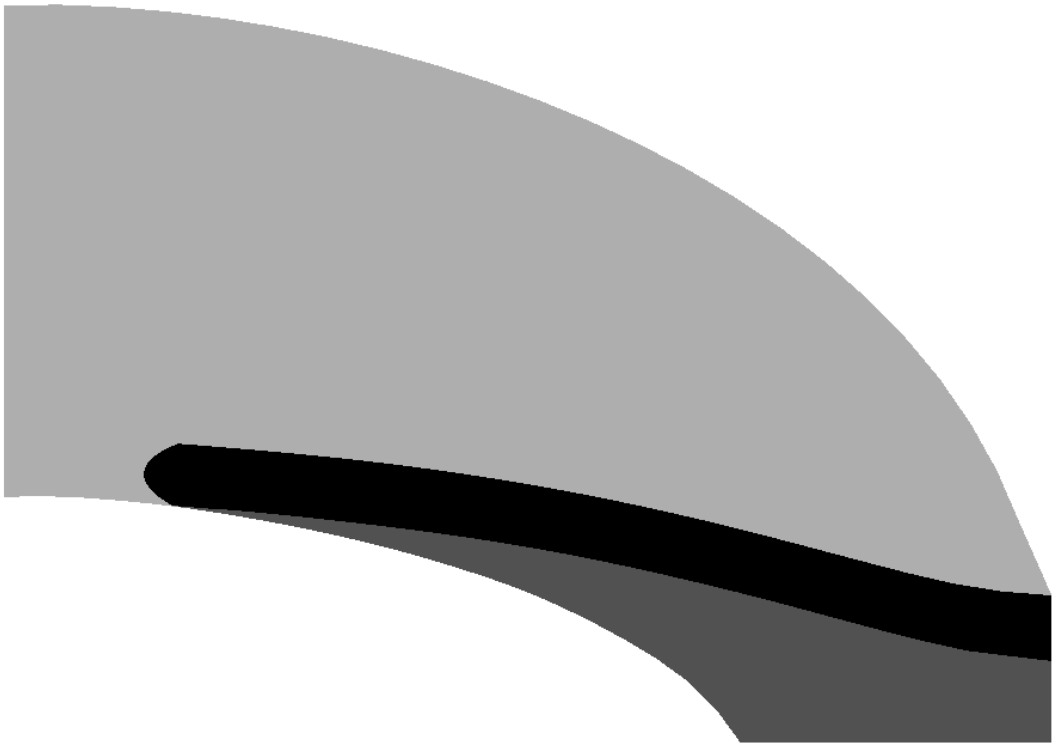

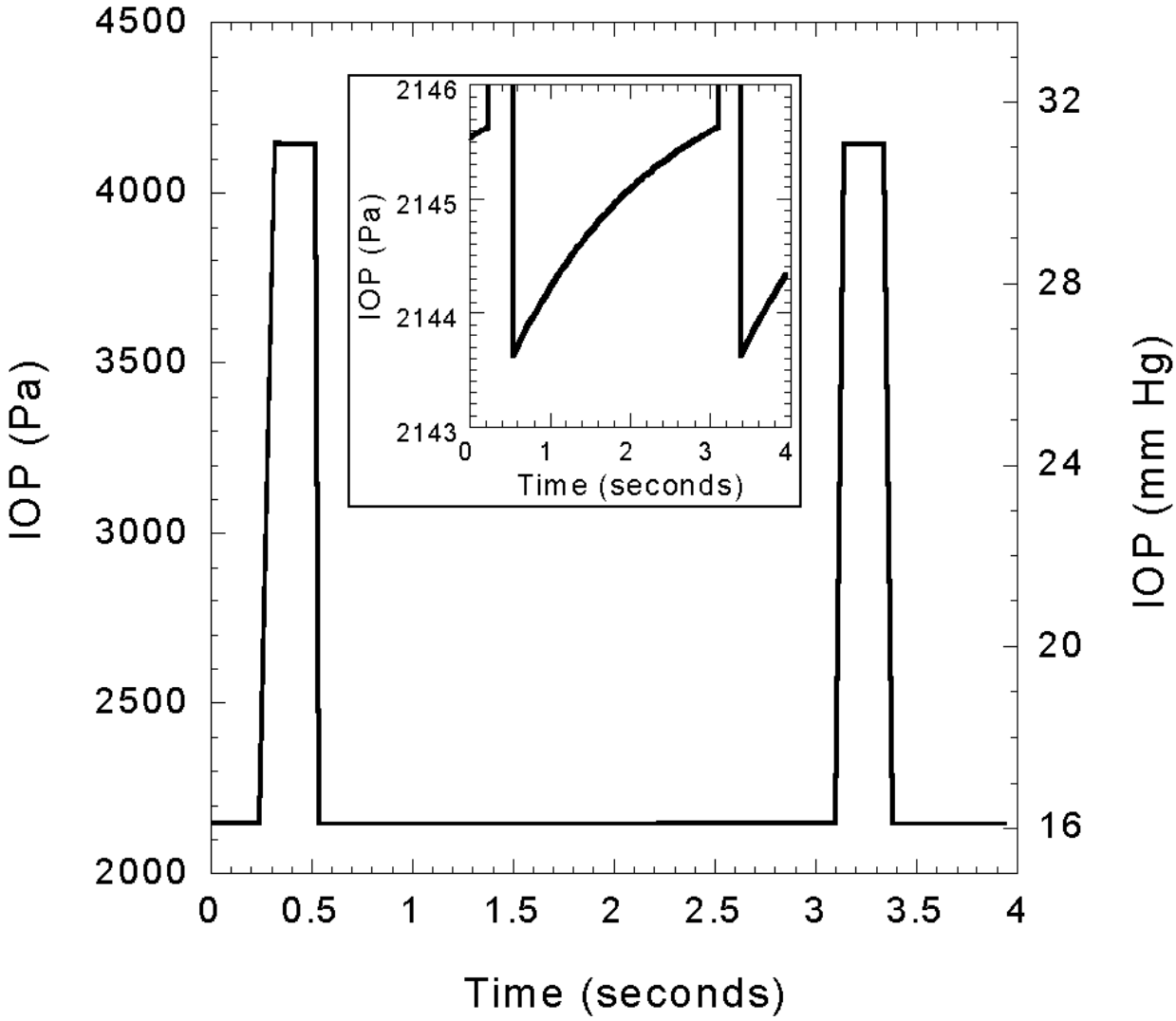
4500
4000
3500
3000
2500
2000
IOP (Pa)
0
0.5
1
1.5
2
2.5
3
3.5
4
Time (seconds)
32
28
24
20
16
IOP (mm Hg)
2146
2145
2144
2143
IOP (Pa)
0
1
2
3
4
Time (seconds)

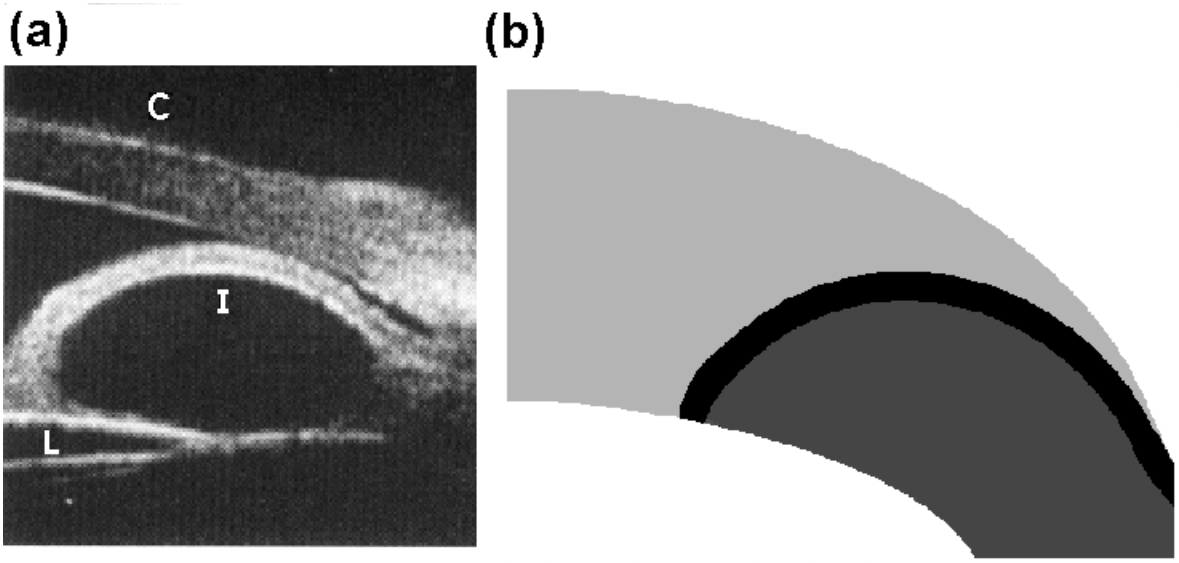
(a)
C
I
L
(b)